PHYSICAL REVIEW APPLIED **6,** 054009 (2016)

Offset-Free Gigahertz Midinfrared Frequency Comb Based on Optical Parametric Amplification in a Periodically Poled Lithium Niobate Waveguide

A. S. Mayer,[1] C. R. Phillips,[1] C. Langrock,[2] A. Klenner,[3,1] A. R. Johnson,[3,4] K. Luke,[5] Y. Okawachi,[3]
M. Lipson,[6] A. L. Gaeta,[3] M. M. Fejer,[2] and U. Keller[1]
[1]*Department of Physics, Institute for Quantum Electronics, ETH Zurich, CH-8093 Zurich, Switzerland*
[2]*Edward L. Ginzton Laboratory, Stanford University, Stanford, California 94305, USA*
[3]*Applied Physics and Applied Mathematics, Columbia University, New York, New York 10027, USA*
[4]*School of Applied and Engineering Physics, Cornell University, Ithaca, New York 14853, USA*
[5]*School of Electrical and Computer Engineering, Cornell University, Ithaca, New York 14853, USA*
[6]*Department of Electrical Engineering, Columbia University, New York, New York 10027, USA*

(Received 30 August 2016; revised manuscript received 18 October 2016; published 18 November 2016)

We report the generation of an optical-frequency comb in the midinfrared region with 1-GHz comb-line spacing and no offset with respect to absolute-zero frequency. This comb is tunable from 2.5 to 4.2 μm and covers a critical spectral region for important environmental and industrial applications, such as molecular spectroscopy of trace gases. We obtain such a comb using a highly efficient frequency conversion of a near-infrared frequency comb. The latter is based on a compact diode-pumped semiconductor saturable absorber mirror–mode-locked ytterbium-doped calcium-aluminum gadolynate (Yb:CALGO) laser operating at 1 μm. The frequency-conversion process is based on optical parametric amplification (OPA) in a periodically poled lithium niobate (PPLN) chip containing buried waveguides fabricated by reverse proton exchange. The laser with a repetition rate of 1 GHz is the only active element of the system. It provides the pump pulses for the OPA process as well as seed photons in the range of 1.4–1.8 μm via supercontinuum generation in a silicon-nitride (Si_3N_4) waveguide. Both the PPLN and Si_3N_4 waveguides represent particularly suitable platforms for low-energy nonlinear interactions; they allow for mid-IR comb powers per comb line at the microwatt level and signal amplification levels up to 35 dB, with 2 orders of magnitude less pulse energy than reported in OPA systems using bulk devices. Based on numerical simulations, we explain how high amplification can be achieved at low energy using the interplay between mode confinement and a favorable group-velocity mismatch configuration where the mid-IR pulse moves at the same velocity as the pump.

DOI: 10.1103/PhysRevApplied.6.054009

I. INTRODUCTION

The midinfrared spectral region between 2 and 20 μm covers the strong vibrational transitions of a variety of molecules that play an important role in environmental, medical, and industrial diagnostics. The ability to detect and quantify the presence of such molecules or to investigate their properties on a more fundamental level is thus directly linked to the availability of a light source capable of probing these transitions. Laser-frequency combs—i.e., lasers whose spectra consist of a series of equally spaced discrete optical lines—combine three essential assets: the high brightness of the light leads to a high detection sensitivity, the narrow linewidth of the individual comb lines allows for high-resolution measurements, while the large spectral bandwidth enables fast simultaneous detection of multiple species.

The success of optical-frequency combs in the near-infrared region has been strongly tied to the advancement of mode-locked lasers in that wavelength range [1–5]. Well-established gain media include Ti:sapphire [6] emitting around 800 nm, and various host crystals doped with ytterbium (Yb) or erbium (Er) emitting in the 1- and 1.5-μm regions, respectively [7–9]. Various approaches have recently been pursued to extend the spectral coverage of frequency combs into the midinfrared region [10]. Direct approaches include alternative laser gain materials for mode-locked solid-state and fiber lasers [11–13] or semiconductor devices such as quantum-cascade lasers [14,15]. Another approach relies on exploiting different aspects of nonlinear optics, such as supercontinuum generation (SCG) in fibers [16–18] and waveguides [19–21], or Kerr-comb generation in microresonators [22,23].

The challenge these approaches have in common is the difficulty to detect and control the comb offset frequency [24–26], i.e., the parameter that defines the exact position of the evenly spaced frequency-comb lines on the absolute-frequency axis. This problem can be circumvented by difference-frequency generation (DFG): in this nonlinear process, the low-frequency part of a comb (termed the “signal”) is mixed with the high-frequency components (the “pump”) of the same comb in a medium exhibiting a second-order ($\chi^{(2)}$) nonlinearity, resulting in

© 2016 American Physical Society

a difference-frequency comb (the "idler") which will be offset-free [27].

A configuration where the signal gets significantly amplified during this mixing process is known as an optical parametric amplifier (OPA). DFG- and OPA-based mid-IR frequency combs have already been demonstrated using bulk devices of various materials, such as periodically poled lithium niobate (PPLN) [28–32], GaSe [33], $AgGaSe_2$ [34], $CdSiP_2$ [35], and orientation-patterned GaAs [36]. Because of the limited interaction length caused by diffraction and material dispersion, single-pass bulk OPAs typically require watt-level pump beams and several hundreds of milliwatts of initial signal power to achieve powers per comb line >1 μW in the mid-IR region. Schemes based on high-power oscillators [37], laser preamplification of a pump and/or signal beam [38], or an intracavity OPA [39] have been demonstrated. Higher efficiencies in converting a near-IR frequency comb to the mid-IR region can be obtained in a resonant cavity, i.e., by turning the OPA into an optical parametric oscillator [40–45]. However, the passive comb-offset stability will be lost and the implementation of an active stabilization [46] is instead required to eliminate the offset. The development of stabilized mid-IR frequency combs therefore benefits from a robust and compact configuration that allows for efficient frequency conversion at low energies with passive comb-offset stabilization, using a single mode-locked laser oscillator as the only active medium.

Here, we demonstrate chip-scale waveguide technology as a compact low-energy platform for generating widely tunable, offset-free mid-IR frequency combs. A diode-pumped solid-state laser operating at 1 μm with a repetition rate of 1 GHz serves as a single active source with two output beams. While one beam is directly used to pump an OPA process in a PPLN waveguide, the other is spectrally broadened in a silicon-nitride (Si_3N_4) waveguide to generate signal photons in the wavelength range of 1.4–1.8 μm. The idler can be tuned from 2.5 to 4.2 μm by laterally translating the PPLN chip across waveguides with varying quasi-phase-matching (QPM) periods [47]. With just 300 pJ of pump-pulse energy and initial seed powers of <20 nW per comb line, we achieve microwatt-level comb-line powers in the mid-IR region. Compared to systems based on nonlinear fibers for SCG and bulk PPLN for the OPA process [38], the required pulse energy for obtaining the same power per comb line is lowered by nearly 2 orders of magnitude.

In the following, we provide the details of the experimental setup, present the mid-IR comb results, and explain via numerical simulations how the approach leverages favorable aspects of the waveguide dispersion in order to maximize the achievable OPA gain. Moreover, our simulations, which are in excellent agreement with our experimental results, show that waveguides offer the possibility to enter high-gain OPA regimes that are inaccessible to bulk devices at low energies. The ability to perform efficient supercontinuum-seeded frequency conversion at low pulse energies, as demonstrated and explained here, could enable multigigahertz comb-resolved sources based on chip-scale nonlinear-optical devices, directly driven by highly compact laser oscillators, thereby removing the need for laser amplifiers and bulk frequency converters in such systems.

II. EXPERIMENTAL SETUP

The passively mode-locked laser oscillator shown in Fig. 1(a) consists of a 2-mm-long ytterbium-doped calcium-aluminum gadolynate (Yb∶CALGO) [48] emitting at 1053 nm and pumped at 980 nm using a spatially multimode pump diode. The laser is mode locked with a semiconductor saturable absorber mirror (SESAM) [49] and can produce pulses as short as 63 fs at a repetition rate of 1.025 GHz, with an output power of up to 1.7 W (when both output beams are combined) [50]. One of the output beams is coupled to a 7.5-mm-long Si_3N_4 waveguide (spiraled onto a square of 1 × 1 mm) with a cross section of 690 × 900 nm [Fig. 1(b)] [51–53]. A coupled pulse

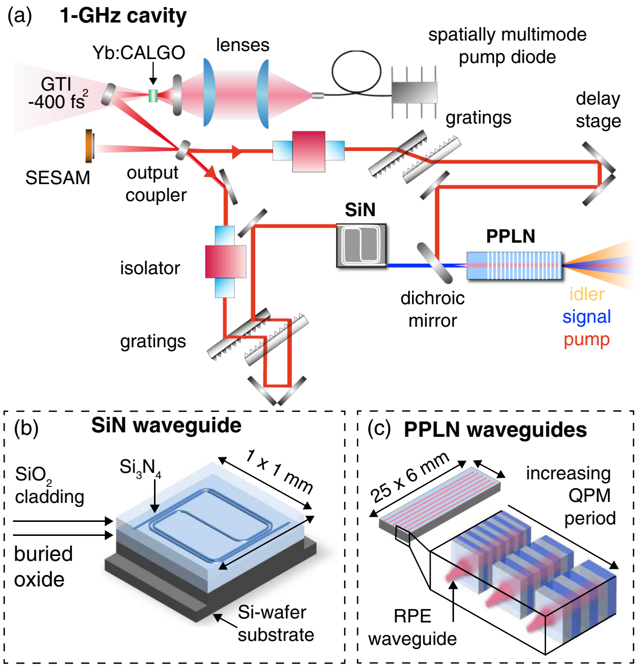

FIG. 1. (a) Experimental setup showing the two output beams of the 1-GHz laser cavity. The negative second-order intracavity dispersion necessary to achieve soliton mode locking is provided by a Gires-Tournois-interferometer- (GTI-)type mirror. Isolators prevent potential back reflections from the waveguide facets into the laser. Grating pairs are used to compensate for the isolator dispersion and additionally stretch the pulse in the OPA pump arm. (b) Sketch of the (1 × 1)-mm chip with the 7.5-mm-long Si_3N_4 waveguide embedded in silicon dioxide (SiO_2). (c) Excerpt of the PPLN chip containing buried RPE waveguides in regions with different poling periods. The first 6.5 mm of the 2.5-cm-long chip are unpoled, and the waveguides are tapered to facilitate single-mode coupling.

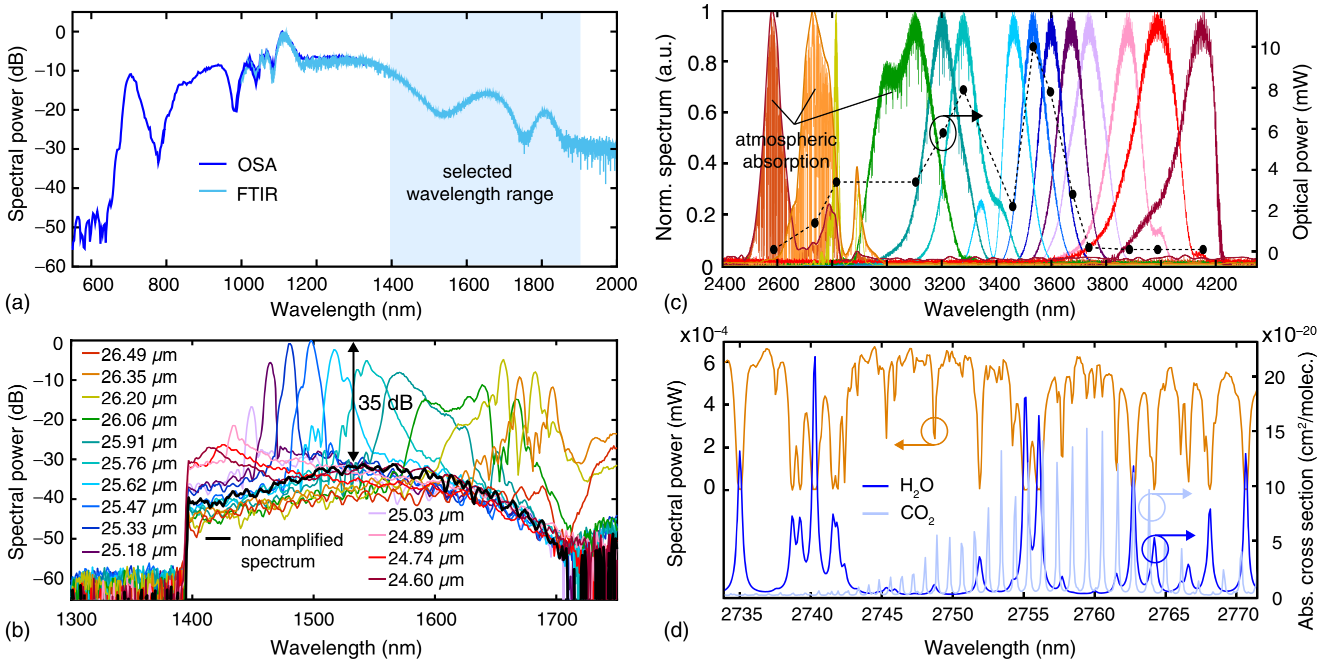

FIG. 2. (a) Supercontinuum obtained with 40 pJ of coupled pulse energy in the Si_3N_4 waveguide. The shaded part is used as a signal input for the OPA. (b) Scan of the amplified signal spectra obtained by laterally scanning the chip across the different QPM periods, recorded with a grating-based optical spectrum analyzer (OSA). (c) Normalized mid-IR spectra recorded with a Fourier-transform infrared spectrometer (FTIR) ranging from 2.5 to 4.2 μm and corresponding to the amplified signal spectra shown in (b). The right axis displays the absolute power levels, with a maximum of 10 mW at 3.55 μm. The power drop near 3.45 μm is due to a slight defect in this particular waveguide, resulting in less overall transmitted power. (d) Enlargement of an FTIR trace recorded with instrument-limited resolution of 3.6 GHz using the free-space port after approximately 1 m of propagation in air (orange) and absorption cross sections of water (dark blue) and carbon dioxide (light blue) taken from the HITRAN database.

energy of 40 pJ (coupling efficiency 15%) is sufficient to obtain a supercontinuum spanning from 650 to 1800 nm, as shown in Fig. 2(a). Using a long-pass filter, the spectrum is cut at 1400 nm and sent into the PPLN waveguide as a seed for the OPA process.

The PPLN-waveguide chip with a dimension of $25 \times 6 \times 0.5$ mm contains 90 waveguides fabricated by reverse proton exchange (RPE). The RPE method exhibits a first step of exchanging lithium ions with protons, using a diffusion process to create a region with a higher refractive index capable of guiding light. In order to obtain buried waveguides that support Gaussian modes and efficient nonlinear mixing, the protons near the surface are subsequently removed in a reverse-proton-exchange step. The RPE waveguides used here are fabricated with a 12 μm width and an exchange depth of 2.3 μm. This depth, which is larger than in typical PPLN waveguides designed for telecom applications [54], is chosen in order to guide the mid-IR wavelengths. At the input side of the waveguide, the width of the lithography-mask pattern is adiabatically tapered to 2 μm to allow for efficient and single-mode coupling of the input near-IR beams. The different waveguides are periodically poled, with poling periods ranging from 17 to 30 μm to achieve QPM. Coupling into both waveguides as well as beam collimation at the output is performed in free space using antireflection-coated lenses.

A Faraday isolator protects the laser cavity from potential back reflections from the waveguide facets. Grating pairs are used to compensate for the dispersion introduced by the isolators. Angled waveguide facets could be used in the future to eliminate the isolators. While the pulse at the input of the Si_3N_4 waveguide is recompressed to a nearly-transform-limited 85 fs, the pulses in the pump arm are purposely stretched to nearly 800 fs to maximize the pump-signal interaction in the PPLN waveguide. The general advantage of pump-pulse stretching in a waveguide configuration is discussed in Sec. IV.

III. RESULTS

A. Amplification and mid-IR spectra

Amplified spectra, obtained by scanning through the waveguides with QPM periods from 24.60 to 26.49 μm, are shown in Fig. 2(b). With a maximum pump-average power of 310 mW coupled into the PPLN waveguides, we are able to amplify the spectral region from 1.4 to 1.8 μm obtained by SCG in the Si_3N_4 waveguide by up to 35 dB. The corresponding mid-IR idler spectra range from 2.5 to 4.2 μm, with an average power reaching 10 mW at 3.5 μm [Fig. 2(c)]. Given the comb-line spacing of 1.025 GHz set by the laser, this value corresponds to an average power per comb line of 4 μW. The DFG process leads to passive cancellation of the laser-comb offset; therefore, the stability of the mid-IR comb lines depends only on the stability of the laser repetition rate—and thus the laser-cavity length. Here, sufficient stability is achieved with low-drift mirror mounts and by boxing the setup. By mounting the SESAM on a piezoelectric actuator as described in Ref. [55], such ultrafast laser combs can be fully stabilized with a long-term stabilization loop, and the comb lines can also be shifted by a desired amount.

The amplified signal spectra are recorded with a grating-based optical spectrum analyzer [(OSA), Ando AQ-6315A]. A Fourier-transform infrared spectrometer [(FTIR), Thorlabs OSA2015] is used for the idler spectra. The path length of approximately 1 m between the output of the PPLN waveguide and the free-space input of the FTIR analyzer is sufficient to observe distinctive absorption features in the ambient air. By magnifying the mid-IR comb generated in the waveguide with the QPM period of 26.35 μm [Fig. 2(d)], we can clearly identify the presence of water (H_2O) and carbon-dioxide (CO_2) absorption lines by comparing the spectrum recorded by the FTIR with the corresponding absorption cross sections provided by the high-resolution transmission molecular absorption (HITRAN) database.

B. Noise analysis

The relative intensity noise (RIN) of a frequency comb is an important parameter, as it can limit the achievable signal-to-noise ratio in spectroscopic applications such as dual-comb spectroscopy [56]. In an OPA-based system, the RIN can increase during preamplification of the pump and/or signal, nonlinear broadening steps, and the OPA process itself. RIN characterization at each stage of the setup thus helps us to identify the bottlenecks and, ultimately, to design low-noise systems. Figure 3 shows the RIN in our setup measured at base band using appropriate photodiodes (Silicon Thorlabs PDA100-EC for 980 nm, InGaAs Thorlabs PDA10CS-EC for 1–1.8 μm, HgCdTe VIGO PVI-4TE-6 + MIPDC-5 for 3.5 μm) and a signal-source analyzer (Agilent E5052B). The noise performance of the gigahertz-laser oscillator is set by its multimode pump diode. Since no preamplifier is used, this noise level also corresponds to the RIN of the OPA pump.

To investigate the impact of the OPA process itself, noise measurements are recorded using the waveguide that provides the highest gain and absolute idler power (QPM period 25.47 μm, signal wavelength 1.50 μm). The RIN of the idler is, as expected, very similar to the RIN of the amplified signal. We observed, however, a noise increase of approximately 30 dB with respect to the pump noise level (Fig. 3).

In order to determine the origin of this noise increase, further measurements are performed. We verify that the shot-noise levels, which depend on the wavelength and the optical power of the photodiode, are well below each of the respective RIN measurement results. The measured RIN of the supercontinuum over the full wavelength range accessible by the InGaAs photodiode (1–1.8 μm) is comparable to the gigahertz-laser output, with the exception of white-noise contributions above 100 kHz and technical noise around 100 Hz [Fig. 3, full supercontinuum (SC)]. However, the RIN of the supercontinuum after a 15-nm bandpass filter centered at 1.5 μm is similar to the OPA output (Fig. 3, filtered SC, before OPA). This filter bandwidth is chosen to correspond to the bandwidth of the amplified signal. It is well known that the interplay of the various mechanisms responsible for spectral broadening during the SCG process can lead to strongly-wavelength-dependent RIN [57], which becomes apparent when using narrow-band filters.

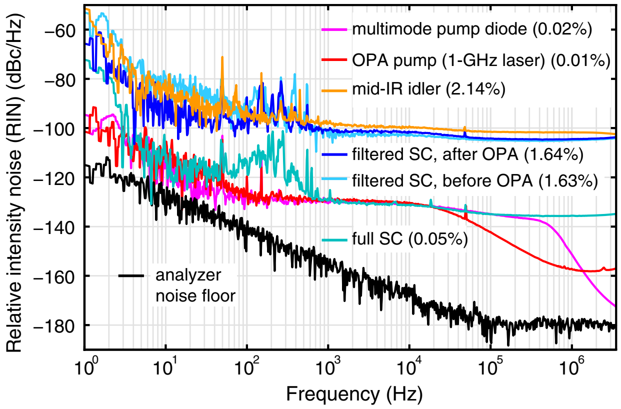

FIG. 3. Relative-intensity-noise (RIN) measurements showing the influence of supercontinuum (SC) generation, supercontinuum filtering, and optical parametric amplification for the waveguide where highest amplification is achieved. The root-mean-square (rms) RIN noise integrated over the interval (1 Hz, 3.5 MHz) is indicated in parentheses for each measurement. The overall noise limit is set by the pump diode of the 1-GHz laser.

We can thus conclude from these observations that, despite the high gain, the OPA process itself is not adding a significant amount of noise, but that the noise increase stems rather from the SCG process in the Si_3N_4 waveguide. In the experiment presented here, the supercontinuum is optimized, above all, for broad bandwidth and spectral coherence [52], but the RIN may be minimized further by numerically analyzing the wavelength dependence of various noise types [58] and adapting the waveguide design accordingly.

IV. DISCUSSION

The experimental OPA results presented above exploit several advantageous properties that waveguides offer in comparison to bulk devices. Simulations in agreement with our experiments will be shown in this section, along with a general discussion on how to take advantage of those waveguide properties to achieve high gain—and thus high conversion efficiency—of a near-IR into a mid-IR comb.

A. Energy-dependent gain

For a phase-matched interaction assuming an undepleted, plane-wave pump field E_p and no initial idler field $[E_i(0) = 0]$, the signal field at the output of an OPA device with length L can be written as [59]

$$E_s(L) = E_s(0)\cosh(\Gamma L), \tag{1}$$

where Γ is the gain parameter defined as

$$\Gamma = \sqrt{\kappa_i \kappa_s}|E_p|, \tag{2}$$

with $\kappa_j = 2\pi d_{\mathrm{eff}}/(n_j \lambda_j)$, $j = i$, s (idler and signal) and where d_{eff} denotes the material-dependent effective nonlinear coefficient.

Assuming sufficiently long pump pulses to provide constant pump intensity for the signal pulse during their interaction, we can approximate the magnitude of the pump field E_p as a function of the peak power $P_{\mathrm{pk}} \sim U_p/\tau_p$:

$$|E_p| \sim \sqrt{\frac{2}{n_p \epsilon_0 c}}\sqrt{\frac{2U_p}{\pi w_0^2 \tau_p}}, \tag{3}$$

where U_p is the pulse energy, τ_p the pulse duration, n_p the refractive index, and w_0 the beam waist. To maximize the interaction in a bulk device, the diffraction length of the beam (and thus the beam radius) is often set to match the distance L_{GVM} over which the pump and signal pulses walk off each other due to group-velocity mismatch (GVM),

$$w_0^2 k_p \approx L_{\mathrm{GVM}} = \tau_p\left(\frac{1}{v_p} - \frac{1}{v_s}\right)^{-1}, \tag{4}$$

where $k_p = n_p 2\pi/\lambda_p$ denotes the pump wave number.

For a given set of phase-matched pump-signal-idler frequencies, the achievable gain will be independent of the pump-pulse duration and can only be scaled via the pulse energy,

$$\Gamma L_{\mathrm{GVM}} \sim C_{p,s,i}\sqrt{U_p} \quad \text{(bulk)}, \tag{5}$$

with a proportionality factor $C_{p,s,i}$ containing the wavelength-dependent material properties. If the pump pulse is too short, then confocal focusing, according to Eq. (4), may yield an intensity above the material damage threshold. In this case, the pump pulse can be stretched to avoid damage. However, the diffraction still limits the achievable gain, according to Eq. (5).

In a waveguide device, however, the interaction is not limited by diffraction anymore, thus eliminating the relation imposed in Eq. (4) for the mode size as a function of GVM. The gain can now additionally be scaled via the pump-pulse duration and the effective mode area A_{eff}, which takes into account the modal overlap inside the waveguide,

$$\Gamma L_{\mathrm{GVM}} \sim C'_{p,s,i}\sqrt{U_p}\sqrt{\frac{\tau_p}{A_{\mathrm{eff}}}} \quad \text{(waveguide)}, \tag{6}$$

where $C'_{p,s,i} = C_{p,s,i}\sqrt{\pi/(2k_p(v_p^{-1} - v_s^{-1}))}$. Thus, high gain can be maintained by stretching the pump-pulse duration despite lowering the pulse energy.

The waveguide cross section is then chosen such as to optimize the overlap of the guided pump, signal, and idler modes (see Sec. III B). Stretching our pump pulses to approximately 800 fs, as described in the experimental section, and taking advantage of the tight mode confinement provided by the PPLN waveguide thus allow us to achieve high gain with nearly one order of magnitude less pulse energy than a best-case estimate of a bulk interaction.

B. Pump versus idler group-velocity mismatch

In the presence of not only GVM between pump and signal but also idler walk-off and group-velocity dispersion of all of the waves, a more-general description of the OPA process is required [60]. In order to explain the gain variations observed experimentally across the broad signal spectral range, we perform numerical simulations based on a general model of the dynamics inside the PPLN waveguides. The model describes the propagation of the pump, signal, and idler pulses through the waveguide, accounting for the wavelength-dependent effective index and modal-overlap coefficients in the waveguide, and it includes both second- and third-order nonlinear properties of the PPLN waveguides [61,62].

In order to determine the dispersion profile of the waveguides, we proceed as follows. First, we simulate the proton diffusion inside the waveguide during the waveguide fabrication process, to obtain a proton concentration profile over the cross section of the waveguide [63]. Following Ref. [63], we obtain the change in refractive index as a function of the wavelength and the transverse position, then calculate the corresponding properties of the fundamental waveguide mode versus the wavelength. These properties are reasonably accurate for IR wavelengths, but less is known about the mid-IR properties. To account for this uncertainty, we apply an additional fixed offset to the effective index for the mid-IR part of the spectrum (wavelengths $> 2\ \mu$m). This offset is chosen such that the numerically predicted set of the phase-matched signal wavelength versus the QPM period is in good agreement with the experimentally measured dependence.

As can be seen in Fig. 4(a), we also include the change in refractive index induced by OH absorption in the material around 2.85 μm [61]. Having calculated the spatial profile of the fundamental mode, an effective area for the OPA process can be defined,

$$A_{\mathrm{eff}}(\omega_p, \omega_s) = \left\{\int_{-\infty}^{0}\int_{-\infty}^{\infty}\bar{d}(x,y)B(x,y,\omega_p)B(x,y,\omega_s) \times B(x,y,\omega_p - w_s)dxdy\right\}^{-2}, \tag{7}$$

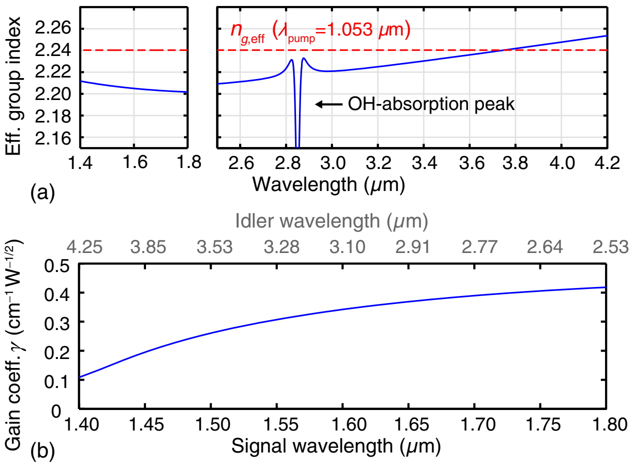

FIG. 4. (a) Effective group index as a function of wavelength over the range used in the experiment. (b) Gain coefficient normalized with respect to power and propagation length. The gain decreases for shorter signal wavelengths as the mode size of the corresponding idler (the gray wavelength scale on top) increases, reducing the modal overlap.

where $\bar{d}$ is a normalized nonlinear coefficient accounting for the so-called dead layer (the layer at the top of the waveguide, where the second-order susceptibility is erased during fabrication) [54], and $B(x, y, \omega)$ is the spatial profile of the fundamental waveguide mode with frequency ω, normalized according to $\int_{-\infty}^{0}\int_{-\infty}^{\infty}|B(x,y,\omega)|^2 dxdy = 1$.

An effective pump intensity, $P_{\mathrm{pk}}/A_{\mathrm{eff}}$, can be introduced, which leads to a normalized OPA gain rate $\gamma = \Gamma/(\sqrt{\text{pump power}})$. Figure 4(b) shows how the modal-overlap integral in Eq. (7) affects the normalized-gain coefficient γ over the range of signal wavelengths used in this experiment.

In order to directly visualize the spectrally dependent effect of modal overlap and GVM on the achievable gain, the pulse-propagation simulations assume a flat-top initial signal spectrum with a flat spectral phase. The following input parameters corresponding to the experimental values are used: 280-mW pump power, 1-mW signal power over the whole flat-top spectrum (1300–1850 nm) and 70-fs pump pulses with a negative chirp of $-25,000\ \mathrm{fs}^2$. A general propagation loss of 0.1 dB/cm is included. We assume a nonlinear coefficient of $d_{33} = 19.5$ pm/V [64] and, to obtain improved agreement with the experimentally measured gain, A_{eff} is scaled by a small factor of 1.17 compared to the directly calculated value from Eq. (7). Without any further adjustments, the simulations (Fig. 5) are able to reproduce remarkably well the features observed in the experiment [Fig. 2(b)].

Looking at the gain curve displayed in Fig. 4(b), one may expect the amplification to monotonically increase with increasing signal wavelength. However, the simulated spectra shown in Fig. 5 are in good agreement with the experimental data presented above: instead of a monotonic increase, a maximal amplification of 35–40 dB is reached in the range of 1450–1500 nm and then a decrease can be observed until the effect of the OH absorption becomes visible for signal wavelengths of around 1650–1700 nm. This trend can be explained as follows: while the gain coefficient γ contains information about the spatial overlap of the idler with the pump and the signal mode inside the waveguide, it does not take into account the temporal behavior of the idler pulses. As can be inferred from Fig. 4(a), the effective group velocity of the idler, $v_{g,\mathrm{eff}}(\lambda_i) = c/n_{\mathrm{group,eff}}(\lambda_i)$, crosses the velocity of the pump (intersection with the red dashed line) when scanning the QPM periods. It is for the signal wavelengths corresponding to this intersection—i.e., where the idler moves at nearly the same velocity as the pump—that we observe maximum signal amplification. Figure 6 illustrates and describes the three regimes that we encounter in the scan:

(1) At a signal wavelength of between 1500 and 1650 nm, both the signal and the idler propagate with a higher velocity than the pump. Although a high spatial overlap is given, the short temporal overlap inhibits further amplification [Fig. 6(a)].

(2) For wavelengths of around 1450–1500 nm, the corresponding idler temporally stays with the pump, leading to the buildup of a strong idler pulse and maximal signal amplification [Fig. 6(b)].

(3) In the third regime (<1450 nm), the signal and the idler have opposite group velocities with respect to the pump [Fig. 6(c)]. This configuration acts as a “trap” for the signal and idler pulses, as they are pulled towards each other, therefore ensuring a long interaction length and, potentially, high amplification. However, the amplification becomes highly suppressed in this wavelength range due to the increasing mode size of the idler and the resulting poor spatial overlap.

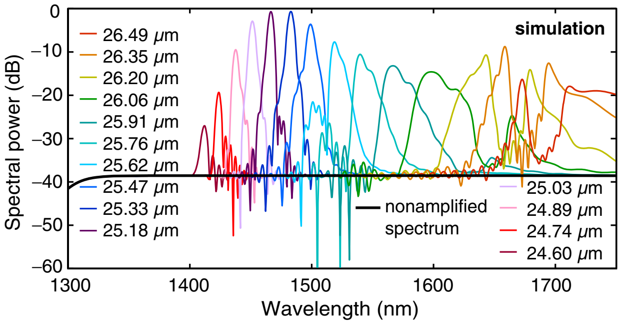

FIG. 5. Simulated amplification of a flat-top signal spectrum (the black line) when scanning through the experimentally used QPM periods.

From these experimental and numerical observations, we conclude that the highest gain—and thus the most efficient mid-IR idler generation—is achieved by designing a waveguide where the idler group velocity is as close as possible to that of the pump while maintaining a high spatial overlap.

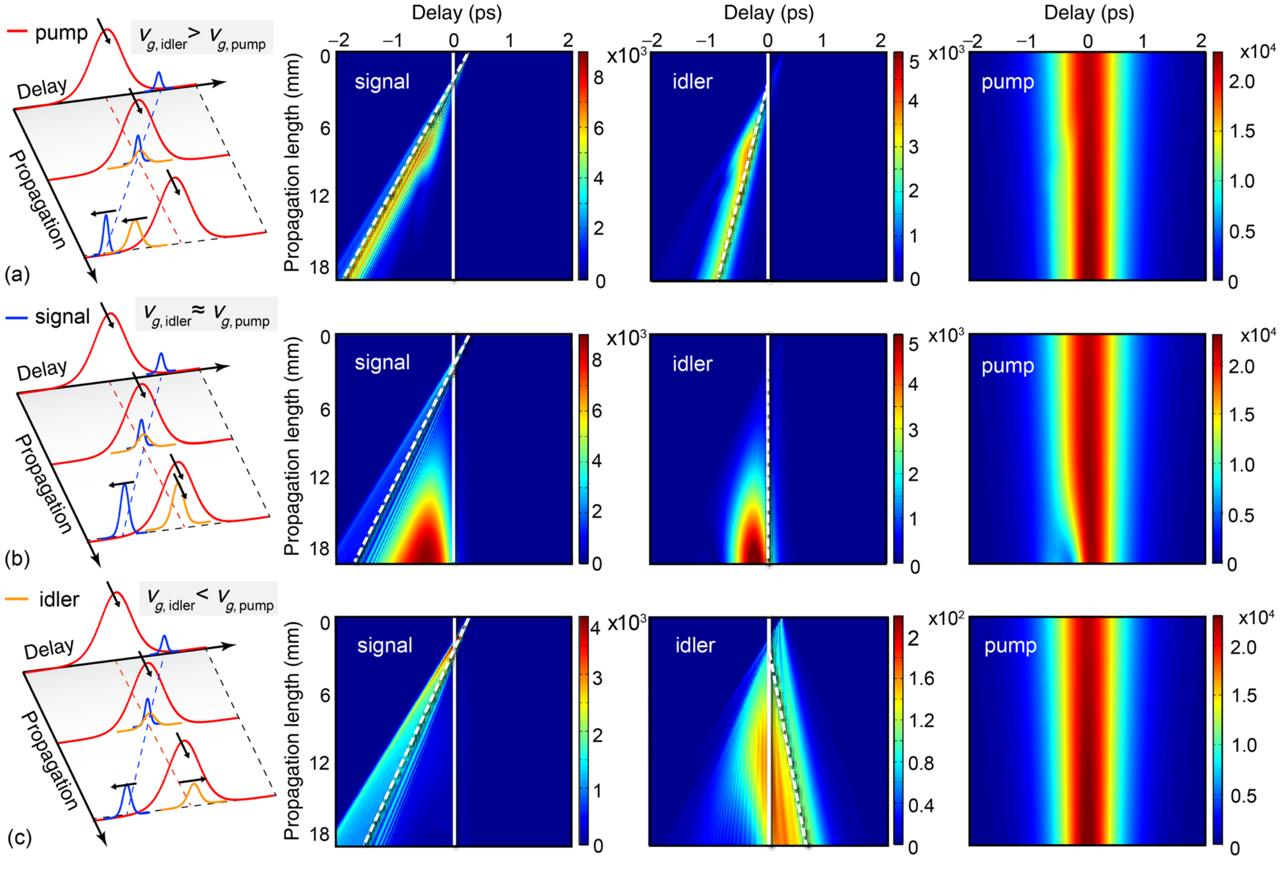

FIG. 6. Illustrative sketch and magnitude of the interacting fields with the center of the pump pulse setting the reference frame for all figures. The dashed white lines indicate the expected temporal lead or lag of signal and idler pulses with respect to the pump due to group-velocity mismatch (GVM). (a) Idler faster than pump. The three pulses overlap over only a short distance: the energy transfer from pump to signal and idler is limited. (b) Idler follows pump. As the signal is passing through the pump pulse, the generated idler photons stay overlapped with the pump and coherently add up to form a strong pulse. (c) Idler slower than pump, i.e., opposite signs for signal and idler. Signal and idler "drag" each other along, leading to a longer interaction with the pump (the "trapped" state). Note the change in magnitude of the electric field (the color bar) compared to (a) and (b). The lower field magnitudes are a consequence of the reduced spatial-mode overlap, which considerably lowers the gain [as shown in Fig. 4(b)].

V. CONCLUSION

In this paper, we address the challenge of nonlinear-optical frequency conversion at low pulse energies with the aim of transferring a 1-GHz frequency comb at 1 μm into the application-relevant mid-IR spectral region. Using a SESAM-mode-locked laser at 1 μm, we have achieved tunable offset-free combs from 2.5 to 4.2 μm with up to 4 μW of power per comb line around 3.5 μm. The comb spectra are generated in a PPLN RPE waveguide by optical parametric amplification. The signal photons for the OPA process are obtained by supercontinuum generation in a silicon-nitride waveguide with only 40 pJ of coupled pulse energy. During the OPA stage, this signal beam is amplified by up to 35 dB using 300 pJ of pump energy. We show that, in contrast to bulk devices, signal amplification in a waveguide OPA can be increased by stretching the pump pulse and exploiting the waveguide dispersion to obtain a similar effective group velocity for pump and idler pulses. Those degrees of freedom provide interesting design opportunities for low-energy frequency conversion of a variety of compact laser sources, including semiconductor lasers [65], without the need for additional laser power amplifiers.

ACKNOWLEDGMENTS

We thank M. Geiser and M. Mangold from IRsweep for their mid-IR photodiode. In addition, the authors acknowledge support of the technology and clean-room facility FIRST of ETH Zurich for advanced micro- and nanotechnology. This work is supported by the Swiss Innovation Promotion Agency with CTI Contract No. 17137.1 PFMN-NM, the DARPA DODOS program through Grant No. N66001-16-1-4055, and the Air Force Office of Scientific Research (AFOSR) (Grants No. FA9550-09-1-0233 and No. FA9550-05-1-0180).

[1] U. Keller, Recent developments in compact ultrafast lasers, Nature (London) **424**, 831 (2003).

[2] W. Sibbett, A. A. Lagatsky, and C. T. A. Brown, The development and application of femtosecond laser systems, Opt. Express **20**, 6989 (2012).

[3] Martin E. Fermann and Ingmar Hartl, Ultrafast fibre lasers, Nat. Photonics **7**, 868 (2013).

[4] Jungwon Kim and Youjian Song, Ultralow-noise mode-locked fiber lasers and frequency combs: Principles, status, and applications, Adv. Opt. Photonics **8**, 465 (2016).

[5] U. Keller, Ultrafast solid-state laser oscillators: A success story for the last 20 years with no end in sight, Appl. Phys. B **100**, 15 (2010).

[6] P. F. Moulton, Spectroscopic and laser characteristics of Ti:Al_2O_3, J. Opt. Soc. Am. B **3**, 125 (1986).

[7] C. Hönninger, R. Paschotta, M. Graf, F. Morier-Genoud, G. Zhang, M. Moser, S. Biswal, J. Nees, A. Braun, G. A. Mourou, I. Johannsen, A. Giesen, W. Seeber, and U. Keller, Ultrafast ytterbium-doped bulk lasers and laser amplifiers, Appl. Phys. B **69**, 3 (1999).

[8] V. P. Gapontsev, S. M. Matitsin, A. A. Isineev, and V. B. Kravchenko, Erbium glass lasers and their applications, Opt. Laser Technol. **14**, 189 (1982).

[9] Federico Pirzio, Matthias Kemnitzer, Annalisa Guandalini, Florian Kienle, Stefano Veronesi, Mauro Tonelli, Juerg Aus der Au, and Antonio Agnesi, Ultrafast, solid-state oscillators based on broadband, multisite Yb-doped crystals, Opt. Express **24**, 11782 (2016).

[10] Albert Schliesser, Nathalie Picque, and Theodor W. Hänsch, Mid-infrared frequency combs, Nat. Photonics **6**, 440 (2012).

[11] E. Sorokin, I. T. Sorokina, J. Mandon, G. Guelachvili, and N. Picqué, Sensitive multiplex spectroscopy in the molecular fingerprint 2.4 μm region with a Cr^{2+}:ZnSe femtosecond laser, Opt. Express **15**, 16540 (2007).

[12] A. A. Lagatsky, P. Koopmann, P. Fuhrberg, G. Huber, C. T. A. Brown, and W. Sibbett, Passively mode locked femtosecond Tm:Sc_2O_3 laser at 2.1 μm, Opt. Lett. **37**, 437 (2012).

[13] Simon Duval, Martin Bernier, Vincent Fortin, Jérôme Genest, Michel Piché, and Réal Vallée, Femtosecond fiber lasers reach the mid-infrared, Optica **2**, 623 (2015).

[14] Andreas Hugi, Gustavo Villares, Stephane Blaser, H. C. Liu, and Jerome Faist, Mid-infrared frequency comb based on a quantum cascade laser, Nature (London) **492**, 229 (2012).

[15] Q. Y. Lu, M. Razeghi, S. Slivken, N. Bandyopadhyay, Y. Bai, W. J. Zhou, M. Chen, D. Heydari, A. Haddadi, R. McClintock, M. Amanti, and C. Sirtori, High power frequency comb based on mid-infrared quantum cascade laser at $\lambda \sim 9$ μm, Appl. Phys. Lett. **106**, 051105 (2015).

[16] Alireza Marandi, Charles W. Rudy, Victor G. Plotnichenko, Evgeny M. Dianov, Konstantin L. Vodopyanov, and Robert L. Byer, Mid-infrared supercontinuum generation in tapered chalcogenide fiber for producing octave-spanning frequency comb around 3 μm, Opt. Express **20**, 24218 (2012).

[17] Christian Rosenberg Petersen, Uffe Møller, Irnis Kubat, Binbin Zhou, Sune Dupont, Jacob Ramsay, Trevor Benson, Slawomir Sujecki, Nabil Abdel-Moneim, Zhuoqi Tang, David Furniss, Angela Seddon, and Ole Bang, Mid-infrared supercontinuum covering the 1.4–13.3 μm molecular fingerprint region using ultra-high NA chalcogenide step-index fibre, Nat. Photonics **8**, 830 (2014).

[18] Yi Yu, Xin Gai, Ting Wang, Pan Ma, Rongping Wang, Zhiyong Yang, Duk-Yong Choi, Steve Madden, and Barry Luther-Davies, Mid-infrared supercontinuum generation in chalcogenides, Opt. Mater. Express **3**, 1075 (2013).

[19] Ryan K. W. Lau, Michael R. E. Lamont, Austin G. Griffith, Yoshitomo Okawachi, Michal Lipson, and Alexander L. Gaeta, Octave-spanning mid-infrared supercontinuum generation in silicon nanowaveguides, Opt. Lett. **39**, 4518 (2014).

[20] Neetesh Singh, Darren D. Hudson, Yi Yu, Christian Grillet, Stuart D. Jackson, Alvaro Casas-Bedoya, Andrew Read, Petar Atanackovic, Steven G. Duvall, Stefano Palomba, Barry Luther-Davies, Stephen Madden, David J. Moss, and Benjamin J. Eggleton, Midinfrared supercontinuum generation from 2 to 6 μm in a silicon nanowire, Optica **2**, 797 (2015).

[21] Bart Kuyken, Takuro Ideguchi, Simon Holzner, Ming Yan, Theodor W. Hänsch, Joris Van Campenhout, Peter Verheyen, Stéphane Coen, Francois Leo, Roel Baets, Gunther Roelkens, and Nathalie Picqué, An octave-spanning mid-infrared frequency comb generated in a silicon nanophotonic wire waveguide, Nat. Commun. **6**, 6310 (2015).

[22] C. Y. Wang, T. Herr, P. Del'Haye, A. Schliesser, J. Hofer, R. Holzwarth, T. W. Hänsch, N. Picqué, and T. J. Kippenberg, Mid-infrared optical frequency combs at 2.5 μm based on crystalline microresonators, Nat. Commun. **4**, 1345 (2013).

[23] Austin G. Griffith, Ryan K. W. Lau, Jaime Cardenas, Yoshitomo Okawachi, Aseema Mohanty, Romy Fain, Yoon Ho Daniel Lee, Mengjie Yu, Christopher T. Phare, Carl B. Poitras, Alexander L. Gaeta, and Michal Lipson, Silicon-chip mid-infrared frequency comb generation, Nat. Commun. **6**, 6299 (2015).

[24] H. R. Telle, G. Steinmeyer, A. E. Dunlop, J. Stenger, D. H. Sutter, and U. Keller, Carrier-envelope offset phase control: A novel concept for absolute optical frequency measurement and ultrashort pulse generation, Appl. Phys. B **69**, 327 (1999).

[25] S. A. Diddams, D. J. Jones, J. Ye, S. T. Cundiff, J. L. Hall, J. K. Ranka, R. S. Windeler, R. Holzwarth, T. Udem, and T. W. Hänsch, Direct Link between Microwave and Optical Frequencies with a 300 THz Femtosecond Laser Comb, Phys. Rev. Lett. **84**, 5102 (2000).

[26] D. J. Jones, S. A. Diddams, J. K. Ranka, A. Stentz, R. S. Windeler, J. L. Hall, and S. T. Cundiff, Carrier-envelope phase control of femtosecond mode-locked lasers and direct optical frequency synthesis, Science **288**, 635 (2000).

[27] V. Petrov, F. Rotermund, and F. Noak, Generation of high-power femtosecond light pulses at 1 kHz in the mid-infrared spetral range between 3 and 12 μm by second-order nonlinear processes in optical crystals, J. Opt. A **3**, R1 (2001).

[28] C. Erny, K. Moutzouris, J. Biegert, D. Kühlke, F. Adler, A. Leitenstorfer, and U. Keller, Mid-infrared difference-frequency generation of ultrashort pulses tunable between 3.2 and 4.8 μm from a compact fiber source, Opt. Lett. **32**, 1138 (2007).

[29] Samuel A. Meek, Antonin Poisson, Guy Guelachvili, Theodor W. Hänsch, and Nathalie Picqué, Fourier transform

spectroscopy around 3 μm with a broad difference frequency comb, Appl. Phys. B **114**, 573 (2014).

[30] Feng Zhu, Holger Hundertmark, Alexandre A. Kolomenskii, James Strohaber, Ronald Holzwarth, and Hans A. Schuessler, High-power mid-infrared frequency comb source based on a femtosecond Er:fiber oscillator, Opt. Lett. **38**, 2360 (2013).

[31] Tyler W. Neely, Todd A. Johnson, and Scott A. Diddams, High-power broadband laser source tunable from 3.0 μm to 4.4 μm based on a femtosecond Yb:fiber oscillator, Opt. Lett. **36**, 4020 (2011).

[32] Joachim Krauth, Andy Steinmann, Robin Hegenbarth, Matteo Conforti, and Harald Giessen, Broadly tunable femtosecond near- and mid-IR source by direct pumping of an OPA with a 41.7 MHz Yb:KGW oscillator, Opt. Express **21**, 11516 (2013).

[33] Axel Ruehl, Alessio Gambetta, Ingmar Hartl, Martin E. Fermann, Kjeld S. E. Eikema, and Marco Marangoni, Widely-tunable mid-infrared frequency comb source based on difference frequency generation, Opt. Lett. **37**, 2232 (2012).

[34] David G. Winters, Philip Schlup, and Randy A. Bartels, Subpicosecond fiber-based soliton-tuned mid-infrared source in the 9.7–14.9 μm wavelength region, Opt. Lett. **35**, 2179 (2010).

[35] D. Sánchez, M. Hemmer, M. Baudisch, K. Zawilski, P. Schunemann, H. Hoogland, R. Holzwarth, and J. Biegert, Broadband mid-IR frequency comb with $CdSiP_2$ and $AgGaS_2$ from an Er,Tm:Ho fiber laser, Opt. Lett. **39**, 6883 (2014).

[36] C. R. Phillips, J. Jiang, C. Mohr, A. C. Lin, C. Langrock, M. Snure, D. Bliss, M. Zhu, I. Hartl, J. S. Harris, M. E. Fermann, and M. M. Fejer, Widely tunable midinfrared difference frequency generation in orientation-patterned GaAs pumped with a femtosecond Tm-fiber system, Opt. Lett. **37**, 2928 (2012).

[37] Tobias Steinle, Andy Steinmann, Robin Hegenbarth, and Harald Giessen, Watt-level optical parametric amplifier at 42 MHz tunable from 1.35 to 4.5 μm coherently seeded with solitons, Opt. Express **22**, 9567 (2014).

[38] Flavio C. Cruz, Daniel L. Maser, Todd Johnson, Gabriel Ycas, Andrew Klose, Fabrizio R. Giorgetta, Ian Coddington, and Scott A. Diddams, Mid-infrared optical frequency combs based on difference frequency generation for molecular spectroscopy, Opt. Express **23**, 26814 (2015).

[39] I. Galli, F. Cappelli, P. Cancio, G. Giusfredi, D. Mazzotti, S. Bartalini, and P. De Natale, High-coherence mid-infrared frequency comb, Opt. Express **21**, 28877 (2013).

[40] Florian Adler, Kevin C. Cossel, Michael J. Thorpe, Ingmar Hartl, Martin E. Fermann, and Jun Ye, Phase-stabilized, 1.5 W frequency comb at 2.8–4.8 μm, Opt. Lett. **34**, 1330 (2009).

[41] Zhaowei Zhang, Tom Gardiner, and Derryck T. Reid, Mid-infrared dual-comb spectroscopy with an optical parametric oscillator, Opt. Lett. **38**, 3148 (2013).

[42] Ville Ulvila, C. R. Phillips, Lauri Halonen, and Markku Vainio, High-power mid-infrared frequency comb from a continuous-wave-pumped bulk optical parametric oscillator, Opt. Express **22**, 10535 (2014).

[43] Alireza Marandi, Kirk A. Ingold, Marc Jankowski, and Robert L. Byer, Cascaded half-harmonic generation of femtosecond frequency combs in the mid-infrared, Optica **3**, 324 (2016).

[44] M. Vainio and L. Halonen, Mid-infrared optical parametric oscillators and frequency combs for molecular spectroscopy, Phys. Chem. Chem. Phys. **18**, 4266 (2016).

[45] Delphine Descloux, Jean-Baptiste Dherbecourt, Jean-Michel Melkonian, Myriam Raybaut, Jui-Yu Lai, Cyril Drag, and Antoine Godard, Rapidly tunable optical parametric oscillator based on aperiodic quasi-phase matching, Opt. Express **24**, 11112 (2016).

[46] Richard A. McCracken, Jinghua Sun, Christopher G. Leburn, and Derryck T. Reid, Broadband phase coherence between an ultrafast laser and an OPO using lock-to-zero CEO stabilization, Opt. Express **20**, 16269 (2012).

[47] Valdas Pasiskevicius, Gustav Strömqvist, Fredrik Laurell, and Carlota Canalias, Quasi-phase matched nonlinear media: Progress towards nonlinear optical engineering, Opt. Mater. **34**, 513 (2012).

[48] Johan Petit, Philippe Goldner, and Bruno Viana, Laser emission with low quantum defect in $Yb:CaGdAlO_4$, Opt. Lett. **30**, 1345 (2005).

[49] U. Keller, K. J. Weingarten, F. X. Kärtner, D. Kopf, B. Braun, I. D. Jung, R. Fluck, C. Hönninger, N. Matuschek, and J. Aus der Au, Semiconductor saturable absorber mirrors (SESAMs) for femtosecond to nanosecond pulse generation in solid-state lasers, IEEE J. Sel. Top. Quantum Electron. **2**, 435 (1996).

[50] Alexander Klenner, Stéphane Schilt, Thomas Südmeyer, and Ursula Keller, Gigahertz frequency comb from a diode-pumped solid-state laser, Opt. Express **22**, 31008 (2014).

[51] A. S. Mayer, A. Klenner, A. R. Johnson, K. Luke, M. R. E. Lamont, Y. Okawachi, M. Lipson, A. L. Gaeta, and U. Keller, Frequency comb offset detection using supercontinuum generation in silicon nitride waveguides, Opt. Express **23**, 15440 (2015).

[52] Adrea R. Johnson, Aline S. Mayer, Alexander Klenner, Kevin Luke, Erin S. Lamb, Michael R. E. Lamont, Chaitanya Joshi, Yoshitomo Okawachi, Frank W. Wise, Michal Lipson, Ursula Keller, and Alexander L. Gaeta, Octave-spanning coherent supercontinuum generation in a silicon nitride waveguide, Opt. Lett. **40**, 5117 (2015).

[53] Alexander Klenner, Aline S. Mayer, Adrea R. Johnson, Kevin Luke, Michael R. E. Lamont, Yoshitomo Okawachi, Michal Lipson, Alexander L. Gaeta, and Ursula Keller, Gigahertz frequency comb offset stabilization based on supercontinuum generation in silicon nitride waveguides, Opt. Express **24**, 11043 (2016).

[54] A. Galvanauskas, K. K. Wong, K. El Hadi, M. Hofer, M. E. Fermann, D. Harter, M. H. Chou, and M. M. Fejer, Amplification in 1.2–1.7 μm communication window using OPA in PPLN waveguides, Electron. Lett. **35**, 731 (1999).

[55] S. Schilt, V. Dolgovskiy, N. Bucalovic, C. Schori, M. C. Stumpf, G. Di Domenico, S. Pekarek, A. E. H. Oehler, T. Südmeyer, U. Keller, and P. Thomann, Noise properties of an optical frequency comb from a SESAM-mode-locked 1.5-μm solid-state laser stabilized to the 10^{-13} level, Appl. Phys. B **109**, 391 (2012).

[56] Nathan R. Newbury, Ian Coddington, and William Swann, Sensitivity of coherent dual-comb spectroscopy, Opt. Express **18**, 7929 (2010).

[57] K. L. Corwin, N. R. Newbury, J. M. Dudley, S. Coen, S. A. Diddams, B. R. Washburn, K. Weber, and R. S. Windeler, Fundamental amplitude noise limitations to supercontinuum spectra generated in a microstructured fiber, Appl. Phys. B **77**, 269 (2003).

[58] T. Godin, B. Wetzel, T. Sylvestre, L. Larger, A. Kudlinski, A. Mussot, A. Ben Salem, M. Zghal, G. Genty, F. Dias, and J. M. Dudley, Real time noise and wavelength correlations in octave-spanning supercontinuum generation, Opt. Express **21**, 18452 (2013).

[59] R. Baumgartner and R. Byer, Optical parametric amplification, IEEE J. Quantum Electron. **15**, 432 (1979).

[60] A. V. Smith, D. J. Armstrong, and W. J. Alford, Increased acceptance bandwidths in optical frequency conversion by use of multiple walk-off-compensating nonlinear crystals, J. Opt. Soc. Am. B **15**, 122 (1998).

[61] C. R. Phillips, Carsten Langrock, J. S. Pelc, M. M. Fejer, I. Hartl, and Martin E. Fermann, Supercontinuum generation in quasi-phasematched waveguides, Opt. Express **19**, 18754 (2011).

[62] C. R. Phillips, Ph.D. thesis, Stanford University, 2012.

[63] R. V. Roussev, Ph.D. thesis, Stanford University, 2006.

[64] Ichiro Shoji, Takashi Kondo, Ayako Kitamoto, Masayuki Shirane, and Ryoichi Ito, Absolute scale of second-order nonlinear-optical coefficients, J. Opt. Soc. Am. B **14**, 2268 (1997).

[65] Bauke W. Tilma, Mario Mangold, Christian A. Zaugg, Sandro M. Link, Dominik Waldburger, Alexander Klenner, Aline S. Mayer, Emilio Gini, Matthias Golling, and Ursula Keller, Recent advances in ultrafast semiconductor disk lasers, Light Sci. Appl. **4**, e310 (2015).